



## Novel high-performance solid oxide fuel cells with bulk ionic conductance dominated thin-film electrolytes

Feng Han <sup>a,\*</sup>, Robert Mücke <sup>a</sup>, Tim Van Gestel <sup>a</sup>, André Leonide <sup>b</sup>, Norbert H. Menzler <sup>a</sup>, Hans Peter Buchkremer <sup>a</sup>, Detlev Stöver <sup>a</sup>

<sup>a</sup> Institute of Energy and Climate Research (IEK-1), Forschungszentrum Jülich, D-52425 Jülich, Germany

<sup>b</sup> Institute of Materials for Electrical and Electronic Engineering (IWE), Karlsruhe Institute of Technology (KIT), D-76131 Karlsruhe, Germany

### HIGHLIGHTS

- Cost-effective wet-chemical method for manufacturing electrolyte for commercial SOFCs.
- Thin electrolyte films were coated on pre-sintered tape-cast anode substrate  $7.5 \times 7.5 \text{ cm}^2$ .
- Cells with  $1 \mu\text{m}$  gas-tight electrolytes and  $4 \times 4 \text{ cm}^2$  active cathode area showed high OCV value ( $\sim 1.1 \text{ V}$ ).
- New cells demonstrated significantly higher power output than standard cells and reported data.
- With LSCF and LSC cathodes, the cells yielded  $1 \text{ A cm}^{-2}$  and  $1.9 \text{ A cm}^{-2}$  ( $0.7 \text{ V}, 600^\circ\text{C}, \text{H}_2$ ), respectively.

### ARTICLE INFO

#### Article history:

Received 18 November 2011

Received in revised form

18 June 2012

Accepted 27 June 2012

Available online 4 July 2012

#### Keywords:

Solid oxide fuel cell

Power density

Electrolyte

Yttria-stabilized zirconia

### ABSTRACT

The overall performance of ionic conducting electrolyte layers is a key factor for determining the power density of solid oxide fuel cells (SOFCs). The aim of this work is to investigate high performance SOFC electrolyte layers developed in our lab via a low cost wet-chemical processing method. In this paper, SOFCs with bulk ionic conductivity dominated thin-film electrolyte demonstrate superior electrochemical performances. Conventional materials for SOFCs are applied in this work: Ni–YSZ cermet as the anode, yttria-stabilized zirconia (YSZ) as the electrolyte, gadolinia-doped ceria (CGO) as the Sr-diffusion barrier layer, and LSCF or LSC as the cathode. At  $0.7 \text{ V}$  and  $600^\circ\text{C}$ , single cells with an active LSCF and LSC cathode area of  $4 \times 4 \text{ cm}^2$  obtain a power density of  $0.7$  and  $1.4 \text{ W cm}^{-2}$ , respectively. According to electrochemical impedance spectroscopy (EIS), the ohmic resistance of the single cells is almost one order of magnitude lower than the conventionally fabricated SOFCs. Due to the improved performance of the electrolyte, SOFCs are able to deliver high power output at reduced operating temperature and increased cell voltage.

© 2012 Elsevier B.V. All rights reserved.

## 1. Introduction

Solid oxide fuel cells (SOFCs) have demonstrated good potential as direct electrochemical energy converters in high-efficiency and environmentally-friendly power generation applications [1,2]. Operating on gas-tight proton or oxygen ionic conductive ceramic electrolytes, SOFCs operate at high temperatures ( $600$ – $1000^\circ\text{C}$ ) in order to achieve an efficient catalytic activity of the electrodes and sufficient ionic conductivity of the electrolyte [3]. The most important advantages of SOFCs include high electrical efficiency (50–70%) and compatibility with hydrocarbon fuels [4]. However, SOFCs operated at high temperatures also suffer from material

constraints, stress from different thermal expansion during thermo-cycling, high manufacturing costs, and issues regarding long-term stability [5].

Many research groups have tried to lower the operating temperature of SOFCs, as this brings with it many advantages, such as cost reduction and a simplified sealing of the SOFC system [6–10]. Moreover, a high power density can reduce the number of cells in a system with fixed power output, which will additionally decrease the total weight, volume and manufacturing costs. As disadvantages, reducing the operating temperature also decreases the thermally activated transport processes, leading to increased ohmic and electrode polarization losses. When using hydrocarbon fuels at temperatures below  $700^\circ\text{C}$ , coking and metal dusting may arise as serious issues [11]. Up to now, none of the reported attempts has succeeded in realizing a high power density over  $1 \text{ W cm}^{-2}$  on SOFCs

\* Corresponding author. Tel.: +49 2461 615437; fax: +49 2461 612455.

E-mail address: f.han@fz-juelich.de (F. Han).

at a reasonable high cell voltage (>0.7 V) and a low operation temperature (e.g. at 600 °C) [12–14]. Most of the reported results are based on button cells with a typical size of 1–3 cm in diameter, which normally deliver a current density lower than 0.5 W cm<sup>-2</sup> at a terminal voltage of 0.7 V and 600 °C [15,16]. Limited by fuel gas transportation and technical difficulties in sealing of the system, the SOFCs with large size normally deliver even lower output [17,18].

More efficient electrolytes and catalytically effective electrodes are key factors for increasing the power density and lowering the operating temperature [19,20]. Today, zirconia-based ceramics are still the most widely used electrolytes in SOFCs due to their good ionic conductivity, low electronic conductivity and outstanding chemical stability [3,21,22]. At 800 °C, yttria-stabilized zirconia (8 mol% YSZ) shows an ionic conductivity of half that of scandia-stabilized zirconia (9.3 mol% ScSZ), i.e. the ohmic loss of the electrolyte can be decreased by 50% by replacing YSZ with ScSZ. In comparison with conventionally fabricated YSZ electrolytes with a typical thickness of 10 µm, a thin-film YSZ electrolyte with a thickness of 1 µm can reduce the ohmic loss by 90%. For a given electrolyte material with a fixed chemical and phase composition at a certain operation temperature, the total conductivity is determined by the bulk conductivity and the grain boundary conductivity. From an electrical point of view, the grain boundary conductivity of YSZ is at least two orders of magnitude lower than the corresponding bulk conductivity at given temperature [23–25]. Due to the domination of bulk ionic conductivity, the total ionic conductivity of a thin-film electrolyte as thin as its single grain size will be significantly higher than the electrolyte made of the same material with the same thickness but smaller grains. Furthermore, the electrode materials with excellent properties are also favorable for reducing the operating temperature of SOFCs and ensuring high performance. In particular, high electronic conductivity, significant oxygen ion mobility and good electrochemical/catalytic activity in reactions are essential properties for the new generation of cathode materials. The perovskite-structured lanthanum strontium cobalt ferrite (LSCF) and lanthanum strontium cobaltite (LSC), well-known as mixed ionic and electronic conducting (MIEC) materials, have been proven as high-performance cathode materials for intermediate-temperature SOFCs [26–28].

In this work, YSZ was chosen as the electrolyte material. Gas-tight 8YSZ thin-film electrolyte layers ~1 µm in thickness were fabricated on tape-cast substrates via the wet chemical route. The reasons for the significantly improved electrochemical performance of the SOFCs were investigated.

## 2. Experimental

### 2.1. Synthesis and preparation

#### 2.1.1. Substrate

Porous tape-cast NiO/YSZ anode supports were used as substrates. Commercial 8YSZ powder (Unitec Ceramics Ltd., U.K.) and NiO powder (Mallinckrodt Baker Inc., USA) were mixed with a weight ratio of 44:56 for slurry preparation in a solvent mixture of ethanol/methyl ethyl ketone. A commercial dispersant Nuosperse FX9086 (Elementis Specialities Inc., USA), polyvinylbutyral (Clariant AG, Germany) as binder and polyethylene glycol (Solutia Deutschland GmbH, Germany) as plasticizer were additionally added in order to adjust the rheological properties of the slurry. Substrate tapes were cast by a doctor blade process. After a proper drying process, the green substrate tapes with a thickness of approximately 0.6 mm were cut into desired dimensions and calcined at 1230 °C for 1 h with a heating rate of 3 K min<sup>-1</sup> [29,30].

#### 2.1.2. Anode

Electrochemically active anode layer with a NiO/YSZ weight ratio of 44:56 was deposited by a screen printing process. Same commercial NiO and YSZ powders as used for substrate fabrication as described in Section 2.1.1 were applied to prepare a screen-printing paste, which contained terpineol (Fluka Chemie AG, Germany) as solvent, polyvinylpyrrolidone (Fluka Chemie AG, Germany) as dispersant and polyvinylbutyral (Clariant AG, Germany) as binder. The anode layer was dried in air and calcined at 1000 °C for 1 h with a heating rate of 3 K min<sup>-1</sup> [30].

#### 2.1.3. Electrolyte

**2.1.3.1. Preparation of nanosuspension and polymeric sol.** A nanosuspension and a polymeric sol were applied for the deposition of the thin-film electrolyte, as described in literature [31,32]. To prepare the nanosuspension, YSZ nanopowder (Sigma–Aldrich GmbH, Germany) was suspended in 0.05 M HNO<sub>3</sub> solution. The suspension was then mixed in the volume ratio of 4:1 with 0.75 wt % polyvinyl alcohol/PVA (Merck KGaA, Germany) solution.

The 8YSZ sol was prepared by a polymeric sol–gel route: 3 g diethanolamine/DEA (Sigma–Aldrich GmbH, Germany) was first diluted in 40 ml n-propanol, and then added into a zirconium-propoxide and yttrium-butoxide (Sigma–Aldrich GmbH, Germany) mixture diluted in 40 ml n-propanol with a proper Y<sup>3+</sup>:Zr<sup>4+</sup> ratio. After 60 min of stirring, 1.8 ml 1 M HNO<sub>3</sub> was first diluted in 50 ml n-propanol, and then dropped into the DEA modified precursor solution at a speed of 1.5 ml min<sup>-1</sup>.

**2.1.3.2. Electrolyte fabrication.** The nanosuspension was first dip-coated twice on substrates forming a PVA/YSZ hybrid layer, which transformed into a mesoporous YSZ layer with a pore size of less than 10 nm through a calcination process at 500 °C. The polymeric sol was further spin-coated and partly infiltrated into the mesoporous YSZ layers. The polymeric precursor layers transformed into microporous ceramic layers by the same calcination process as mentioned above. The process of coating and calcination was repeated to obtain the desired graded multilayer structure. Finally, all layers were co-sintered at 1400 °C for 5 h with a heating rate of 3 K min<sup>-1</sup> in order to obtain gas-tight electrolyte layers with the desired grain size.

#### 2.1.4. Sr-diffusion barrier layer

A Ce<sub>0.8</sub>Gd<sub>0.2</sub>O<sub>2-δ</sub> (CGO) layer with a thickness of 0.5 µm was additionally applied on top of the YSZ electrolyte via reactive sputtering from a planar metallic target using a commercial physical vapor deposition cluster system CS 400 ES (Von Ardenne Anlagentechnik, Germany) [33,34].

#### 2.1.5. Cathode

La<sub>0.58</sub>Sr<sub>0.40</sub>Fe<sub>0.80</sub>Co<sub>0.20</sub>O<sub>3-δ</sub> (LSCF) and La<sub>0.58</sub>Sr<sub>0.40</sub>CoO<sub>3-δ</sub> (LSC) powders were synthesized using the spray drying method. The cathode layers, with a size of 4 × 4 cm<sup>2</sup> for electrochemical single-cell tests and 1 × 1 cm<sup>2</sup> for electrochemical impedance spectroscopy, were screen printed on the 5 × 5 cm<sup>2</sup> half-cells using ethyl cellulose as the binder and terpineol as the solvent. The LSCF cathode was dried at 60 °C in air and subsequently sintered at 1040 °C for 3 h with a heating rate of 3 K min<sup>-1</sup>. The LSC cathode was calcined at 800 °C for 1 h with a heating rate of 3 K min<sup>-1</sup> to remove the organic binder. The cathode thickness was about 50 µm [33].

## 2.2. Characterization

As a test of the gas tightness of the sintered electrolyte layer, the helium leakage value of the half-cells was measured with a leak

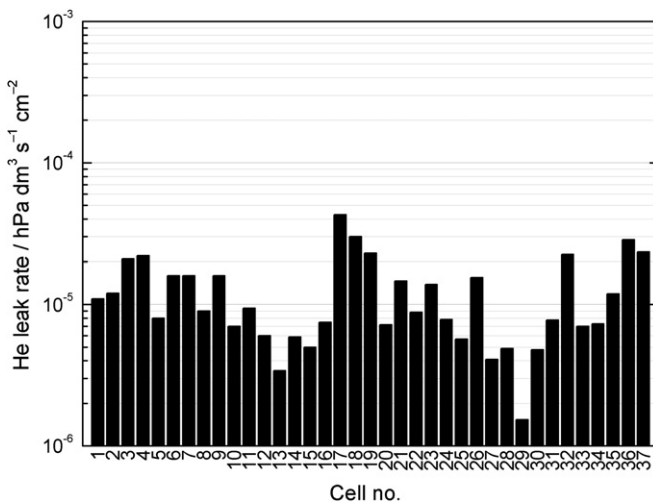


**Fig. 1.** Area-specific helium leak rate of tested half-cells.

rate test module (HTL 260, Pfeiffer Vacuum GmbH, Germany) before the CGO layers and cathode were deposited [35]. The helium flow through the half-cell was determined with a mass spectrometer at a pressure difference of 1000 hPa. The values were normalized to a measured area of  $16 \text{ cm}^2$  and a pressure difference of 100 hPa, which are typical for a SOFC stack. The microstructure of the cells was analyzed by SEM using a Zeiss Gemini Ultra 55 electron microscope (Carl Zeiss NTS GmbH, Germany).

### 2.3. Electrochemistry

#### 2.3.1. Electrochemical single cell test

Electrochemical single cell measurements were performed in the temperature range of 600–900 °C. All measurements were performed with a fuel composition of 97 vol% hydrogen and 3 vol % water with a fuel flow of 1000 standard  $\text{cm}^3 \text{min}^{-1}$  (sccm). The oxidant composition was 21 vol% oxygen and 79 vol% nitrogen with the total flow of 1000 sccm. The electrochemical data were obtained by direct current methods using a Gossen 62N-SSP500-40 current-control power supply (Gossen-Metrawatt GmbH, Germany), and a computer-controlled data recording system (Fluke, Netherlands). The maximum measurable total current of the electrochemical single cell test was limited to 24 A in order to avoid melting of the Pt wires in the set-up, corresponding to a current density of  $1.5 \text{ A cm}^{-2}$  in the case of single cells with a cathode area of  $4 \times 4 \text{ cm}^2$ . The current densities at 0.7 V were calculated using interpolation or linear extrapolation (for current density larger

than  $1.5 \text{ A cm}^{-2}$ ) based on the last five measured data points on the current–voltage plot [26].

#### 2.3.2. Electrochemical impedance spectroscopy (EIS)

Electrochemical impedance spectroscopy (EIS) was carried out on the single cells with an active cathode area of  $1 \times 1 \text{ cm}^2$  and auxiliary electrodes in the gas flow direction in front of and behind the cathode. The data were obtained using a Solartron-1260 frequency response analyzer (Solartron Analytical AMETEK Advanced Measurement Technology GmbH, Germany) in a frequency range from 0.1 Hz to 1 MHz at temperatures from 550 to 900 °C. The fuel gas ( $\text{H}_2$  with 6.0–5.5%  $\text{H}_2\text{O}$ ) and oxidant gas (air) flow rates were maintained at a constant value of 250 sccm during all experiments. The Arrhenius plots of the ohmic resistance and polarization resistances were obtained by analyzing the impedance spectra with a complex nonlinear least-squares (CNLS) approximation method. Based on an accurate analysis of all recorded impedance data and their corresponding distribution function of relaxation times (DRTs), an equivalent circuit model composed of five impedance elements connected in series was applied in interpreting the impedance spectra [36].

## 3. Results and discussion

### 3.1. Helium leakage rate

As can be seen in Fig. 1, the helium leak rate of the half-cells with sintered thin-film electrolytes is in the range of  $1.5 \times 10^{-6}$  to  $4.3 \times 10^{-5} \text{ hPa dm}^3 \text{s}^{-1} \text{cm}^{-2}$ , demonstrating the good gas tightness of the electrolyte layers despite the fact that the electrolytes are as thin as  $\sim 1 \mu\text{m}$ . Most of the cells show lower leak rate than the maximum acceptable value for the Jülich standard cell, i.e.  $2.0 \times 10^{-5} \text{ hPa dm}^3 \text{s}^{-1} \text{cm}^{-2}$  [37]. The thin-film electrolyte layers prepared in this work are proven to be sufficiently dense to separate the fuel gas and air.

### 3.2. SEM

Fig. 2 shows SEM micrographs of the surface and the fracture surface of the electrolyte layers fabricated from a nanosuspension and a polymeric sol. It can be observed in Fig. 2(a) that the grain sizes of the electrolyte are in the nanometer regime after a calcination process at 500 °C for 1 h. As seen in Fig. 2(b), after a sintering process at 1400 °C for 5 h, the nanocrystalline YSZ particles develop into large grains in the micron regime (1–4  $\mu\text{m}$ ). It is notable that most of the grains are flake-shaped and the electrolyte thickness is smaller than the lateral size of the grains. The thin-film YSZ electrolyte with a thickness of  $\sim 1 \mu\text{m}$  appears to be completely dense.

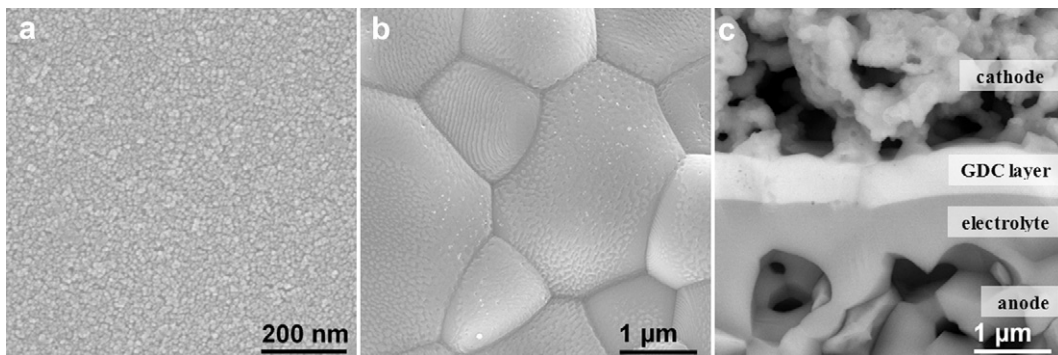


**Fig. 2.** SEM images: (a) surface micrograph of YSZ electrolyte, calcined at 500 °C for 1 h, (b) surface micrograph of YSZ electrolyte, sintered at 1400 °C for 5 h, (c) fracture surface micrograph of single cell (electrochemically tested for 300 h) with a thin-film YSZ electrolyte.

As shown in Fig. 2(c), the electrolyte is found to have a good mechanical, chemical and thermal stability after a 300-h electrochemical single cell test. The thin-film YSZ electrolyte has excellent adherence to the anode substrate with no visible cracks or delamination. No secondary phase, such as ion-blocking Sr-zirconate, is observed at the YSZ/CGO interface, indicating that the CGO Sr-diffusion barrier layer efficiently prevents Sr-diffusion from the LSCF or LSC cathode to the electrolyte.

The fracture surface SEMs and average current densities of three types of cells with different electrolyte/CGO layer combinations are compared in Fig. 3. Single cells with screen-printed electrolyte and CGO layers [38] are denoted as type A cells. Similarly, cells with screen-printed electrolyte layers and physical-vapor-deposited CGO layers [33] are indicated as type B cells. Type A and type B cells are currently standard Jülich cells. The recently developed high-performance cells with nanosuspension dip-coated electrolyte layers ( $\sim 1 \mu\text{m}$  in thickness) are presented as type C cells, which are electrochemically characterized and investigated in this paper.

### 3.3. Electrochemical performance

Demonstrated in Fig. 4, type A cells show the lowest performance due to the following reasons: (1) the thick electrolyte and CGO layers result in a high ohmic resistance, (2) the low sintering density of the CGO layer negatively affects the oxygen ion transportation inside the CGO layer, (3) the porous structure of the screen-printed CGO layer reduced the size of the cathode/CGO and the CGO/electrolyte contacting interfaces, which increased the interfacial resistance, (4) low ionic conductive composite phases form at the CGO/electrolyte interface [33]. In type B cells, the screen-printed CGO layers are replaced with physical-vapor-deposited (PVD) CGO layers and the cell performance is enhanced by reducing the thickness and the resistance of CGO layers, achieving a dense layer structure and avoiding the formation of ion-blocking compounds. In the case of type C cells, the electrochemical performance is further significantly improved by applying the thin-film electrolyte with a dense structure and a remarkably

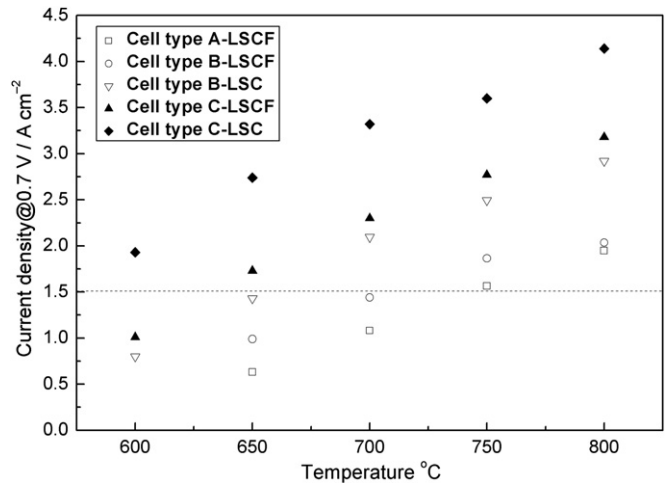


**Fig. 4.** Overview of average current density of cells with different types of electrolyte/CGO layers and cathodes at varied operating temperatures. Current density values below  $1.5 \text{ A cm}^{-2}$  are measured values and the values above  $1.5 \text{ A cm}^{-2}$  were extrapolated based on the measured  $i$ – $V$  plots.

minimized ohmic resistance. Type C cells with a LSCF cathode demonstrate excellent performance and even outperform type B cells with a LSC cathode. The former cells benefited from a remarkably lower ohmic resistance of the thin-film electrolyte, and the latter benefited from the excellent electrochemical properties of the LSC cathode. The maximal power output is realized through superimposing positive effects of all cell components.

As seen in Figs. 4 and 5, type C cells show excellent cell performance. Operated with LSCF cathode, the extrapolated current density is as high as  $3.2 \text{ A cm}^{-2}$  at  $800^\circ\text{C}$  and  $0.7 \text{ V}$ . The power output is significantly higher than that of type A cells with electrolyte layers of  $\sim 10 \mu\text{m}$  in thickness and a CGO layer made by the conventional screen-printing method using microcrystalline powder with the same cell design. At  $600^\circ\text{C}$  and  $0.7 \text{ V}$ , the measured current density is  $1.0 \text{ A cm}^{-2}$  generating a total power

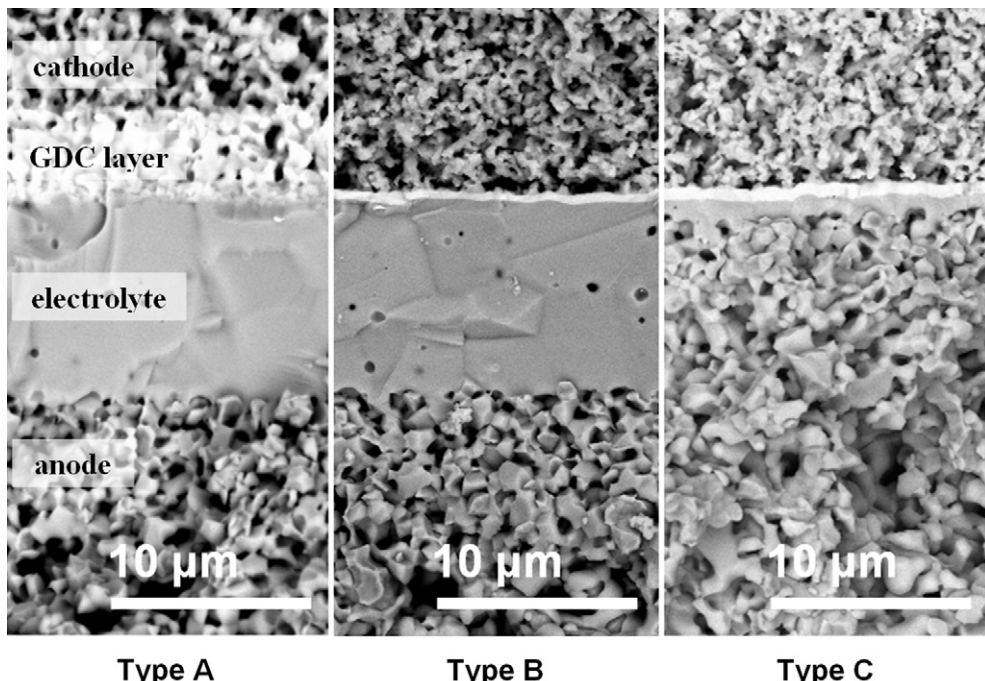


**Fig. 3.** SEM image of cells with different types of electrolyte/CGO layers.

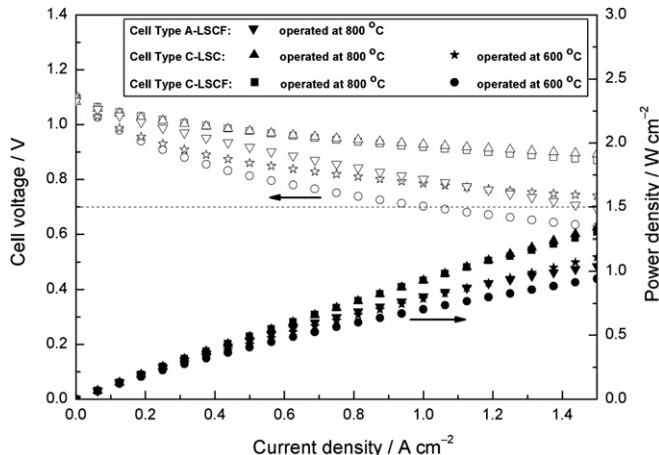


**Fig. 5.** Cell voltage (open symbols) and power density (solid symbols) as a function of current density of fuel cells with a cathode area of  $4 \times 4 \text{ cm}^2$  operated at  $800^\circ\text{C}$  and  $600^\circ\text{C}$ . Cell Type A-LSCF cells consist of conventional  $10 \mu\text{m}$  electrolyte and  $5 \mu\text{m}$  CGO layers, both screen-printed with microcrystalline powders, and LSCF cathode. Type C-LSC and type C-LSCF cells consist of  $1 \mu\text{m}$  thin-film electrolyte deposited with nano-suspension and polymeric sol,  $0.5 \mu\text{m}$  physical-vapor-deposited CGO layers, and LSC or LSCF cathode.

output of  $11.2 \text{ W}$  on a planar SOFC with a  $16 \text{ cm}^2$  LSCF cathode. By using LSC perovskite as the cathode material, the cell performance is further enhanced. An extrapolated current density of  $4.4 \text{ A cm}^{-2}$  and a power density of  $3.1 \text{ W cm}^{-2}$  are derived at  $800^\circ\text{C}$  and  $0.7 \text{ V}$ . The current density of the cells reaches  $1.9 \text{ A cm}^{-2}$  at  $600^\circ\text{C}$  and  $0.7 \text{ V}$ . Type C cells demonstrate significantly high current density in comparison with other reported data of SOFCs with YSZ electrolyte as shown in Table 1. In the temperature range of  $600$ – $800^\circ\text{C}$ , the type C cells investigated in this work outperform not only the cells with thicker electrolyte but also those with similar electrolyte thickness, regardless of the active cathode size.

#### 3.4. Ohmic resistance

The Arrhenius plots of the ohmic resistance ( $R_0$ ) are obtained by analyzing the impedance spectra. As shown in Fig. 6, the ohmic resistances  $R_0$  are  $12, 17, 25, 44, 77$  and  $167 \text{ m}\Omega \text{ cm}^2$  at  $800, 750, 700, 650, 600$  and  $550^\circ\text{C}$ , respectively. These values are one order of magnitude lower than the corresponding values measured on the cells with conventional electrolyte layers ( $\sim 10 \mu\text{m}$  in thickness) and screen-printed CGO layers ( $\sim 5 \mu\text{m}$  in thickness). The ohmic loss of the cell is dominantly determined by the ohmic resistance of the electrolyte, which is dependent on the actual total ionic conductivity of the electrolyte material, the thickness of the electrolyte layer and the operating temperature. As shown in Fig. 7, the YSZ electrolyte layer with a thickness of  $100 \mu\text{m}$  has such a high resistance and ohmic loss that the cells have to be operated at over  $900^\circ\text{C}$  in order

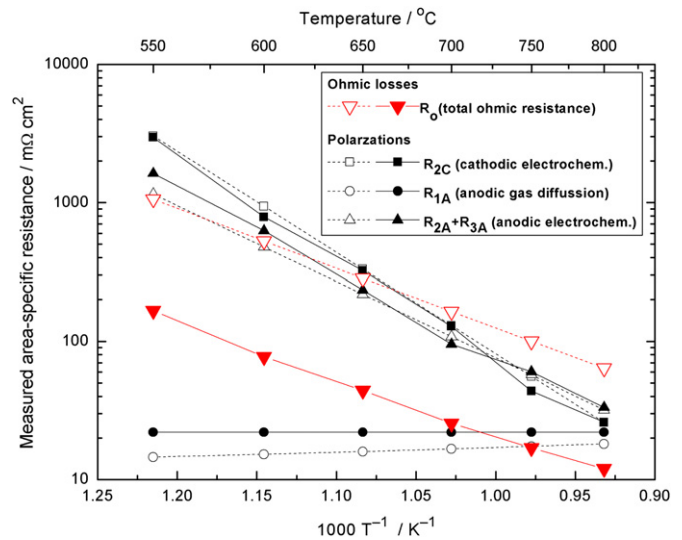


**Fig. 6.** Calculated area-specific resistance of single cells. Dashed line: cells with conventional  $10 \mu\text{m}$  electrolyte and  $5 \mu\text{m}$  CGO layer; solid line: cells with  $1 \mu\text{m}$  thin-film electrolyte and  $0.5 \mu\text{m}$  physical-vapor-deposited CGO layer.

to generate reasonable power output. By reducing the electrolyte thickness to  $10 \mu\text{m}$ , the ohmic resistance significantly decreases and the operating temperature of the cell can be reduced to  $750^\circ\text{C}$ . However, the ohmic loss of a  $10 \mu\text{m}$  thick electrolyte is still too high for the cells to be operated at  $600^\circ\text{C}$  unless the thickness can be further reduced to  $\sim 1 \mu\text{m}$ . The ohmic resistance does not drop much when the electrolyte thickness further decreased from  $1 \mu\text{m}$  to  $0.1 \mu\text{m}$  unless the cells are operated at temperatures below  $550^\circ\text{C}$ . For the thin-film electrolyte prepared in this work, the ionic conductance is not only enhanced by reducing the layer thickness, but also by the domination of high bulk ionic conductivity and minimized grain boundary resistance. As the electrolyte thickness is comparable to the grain thickness, the grain boundary resistance of the electrolyte is negligible. Furthermore, the high currents collected from the cells generate Joule heat and may additionally increase the cell temperature which in turn reduces ohmic and polarization losses during operation [42]. This phenomenon is supposed to have contributed to the lower slope of the  $i$ - $V$  curve of cell type C in comparison to cell type A (Fig. 5). To quantify this effect experimentally in the future, accurate temperature measurements of the cell itself will be necessary.

#### 3.5. Polarization resistance

The polarization resistances of the cells are also shown in Fig. 6.  $R_{2c}$  represents the polarization resistance, which is dependent on the oxygen surface exchange kinetics and  $\text{O}_2^-$  diffusivity on the

**Table 1**  
Current density in comparison with reported data.

Cell	Anode/electrolyte/cathode materials	Electrolyte thickness ( $\mu\text{m}$ )	Active cathode size ( $\text{cm}^2$ )	Current density at $0.7 \text{ V}$ ( $\text{A cm}^{-2}$ )					Reference
				$600^\circ\text{C}$	$650^\circ\text{C}$	$700^\circ\text{C}$	$750^\circ\text{C}$	$800^\circ\text{C}$	
External reference	Ni–YSZ/YSZ/Pt–Pd	0.5	2	0.6	—	—	—	0.9	[15]
External reference	Ni–YSZ/YSZ/LSM–YSZ	20	—	—	—	—	0.8	1.2	[16]
External reference	Ni–YSZ/YSZ/composite	10	81	—	0.6	0.95	—	—	[18]
External reference	Ni–YSZ/YSZ/LSC	1	—	1.1	—	—	—	—	[39]
External reference	Ni–YSZ/YSZ/LSCF–CGO	13	16	—	—	—	0.7	—	[40]
Cell type A-LSCF	Ni–YSZ/YSZ/LSCF	10	16	—	0.6	1.1	1.6	2.1	[38,41]
Cell type B-LSCF	Ni–YSZ/YSZ/LSCF	10	16	—	1.0	1.5	1.9	2.1	[33,34]
Cell type C-LSCF	Ni–YSZ/YSZ/LSCF	1	16	1.0	1.6	2.0	2.5	2.7	—
Cell type C-LSC	Ni–YSZ/YSZ/LSC	1	16	1.9	2.8	3.4	3.8	4.4	—

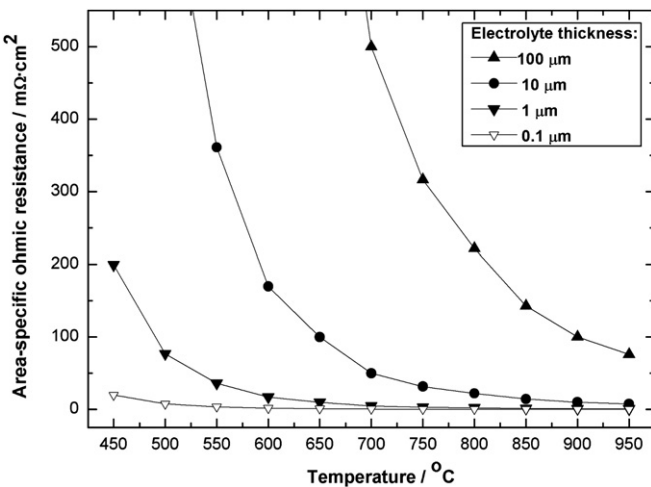


**Fig. 7.** Area-specific ohmic resistance of electrolyte layers with different thicknesses. The calculation is based on the reported conductivity data of 8YSZ [3].

cathode side. The  $R_{2C}$  of cells prepared in this work remain unchanged in comparison with the  $R_{2C}$  value of the conventionally prepared cells. The  $R_{1A}$  and  $(R_{2A} + R_{3A})$  represent the polarization resistance relating to the gas diffusion in the anode and the gas diffusion coupled with a charge transfer reaction and ion transport in the anode layer. The polarization resistance  $R_{1A}$  of the cells with thin-film electrolytes prepared with nanocrystalline particles is slightly higher than that of the cells with electrolytes prepared with microcrystalline particles. In the electrolyte deposition process, the nanocrystalline particles in the nanosuspension may penetrate into the macroporous anode layer and may decrease the pore size and the relative nickel content in the anode layer, which could influence the polarization resistance on the anode side. The  $R_{1A}$  is dependent on the gas diffusion velocity in the anode, which is strongly related to the pore structure of the anode. As the fine YSZ particles infiltrate into the anode reducing its total porosity and pore size, the polarization loss of  $R_{1A}$  slightly increases. In the temperature range of 550–650 °C, the  $R_{2A}$  and  $R_{3A}$  may increase as a result of a decreased gas diffusion rate, or an impeded charge transfer reaction and ionic transport process caused by a decreased Ni/YSZ ratio and a corresponding reduction in active catalytic effects at the triple phase boundaries (TPBs). On the other hand, they may also decrease because of an enlarged electrolyte/anode interface contact area. A dramatic change in the  $R_{2A}$  and  $R_{3A}$  is not observed in the results of the samples tested here. In summary, the total polarization resistance shows no significant difference in all types of cells and it has hardly any influence on the cell performance. Therefore, the most important contribution to the high power output originates from the low ohmic losses of the thin-film electrolyte layers.

#### 4. Conclusions

The ohmic resistance of the electrolyte layer is substantially reduced by reducing electrolyte thickness to ~1 μm and minimizing the grain boundaries along the oxygen transportation path, which is especially favorable for enhancing the performance of SOFCs operated at the intermediate-temperature range. Single cells with an active LSCF or LSC cathode area of  $4 \times 4 \text{ cm}^2$  demonstrate superior high power output, i.e.  $0.7$  or  $1.4 \text{ W cm}^{-2}$  at  $600$  °C for a cell voltage of  $0.7$  V under  $\text{H}_2$  as fuel, which significantly outperform the cells with conventional electrolytes. The achievement of this work has great potentials for building future high-performance SOFC stacks operating at temperature below  $650$  °C,

delivering the same power output as conventional cells operating at above  $700$  °C. The long-term stability of the cells is a subject of further investigation.

#### Acknowledgments

The authors sincerely thank Dr. D. Sebold for the SEM investigations, Dr. V.A.C. Haanappel for the electrochemical single-cell tests, Dr. Sven Uhlenbrück, Frank Vondahlen and Dr. Ronan Nédélec for the PVD depositions, and Dr. Bert de Haart and Dr. Qianli Ma for helpful discussions (all from Forschungszentrum Jülich).

#### References

- B.C.H. Steele, A. Heinzel, *Nature* 414 (2001) 345–352.
- S.C. Singhal, *Solid State Ionics* 152 (2002) 405–410.
- V.V. Kharton, F.M.B. Marques, A. Atkinson, *Solid State Ionics* 174 (2004) 135–149.
- S.C. Singhal, *MRS Bull.* 25 (2000) 16–21.
- F. Tietz, Q. Fu, V.A.C. Haanappel, A. Mai, N.H. Menzler, S. Uhlenbrück, *Int. J. Appl. Ceram. Technol.* 4 (2007) 436–455.
- S.W. Tao, J.T.S. Irvine, *Nat. Mater.* 2 (2003) 320–325.
- Z.P. Shao, S.M. Haile, *Nature* 431 (2004) 170–173.
- C.R. Xia, M.L. Liu, *Adv. Mater.* 14 (2002) 521–523.
- H. Huang, M. Nakamura, P.C. Su, R. Fasching, Y. Saito, F.B. Prinz, *J. Electrochem. Soc.* 154 (2007) B20–B24.
- T. Hibino, A. Hashimoto, K. Asano, M. Yano, M. Suzuki, M. Sano, *Electrochim. Solid State Lett.* 5 (2002) A242–A244.
- V. Alzate-Restrepo, J.M. Hill, *J. Power Sources* 195 (2010) 1344–1351.
- F.B. Prinz, C.C. Chao, C.M. Hsu, Y. Cui, *ACS Nano* 5 (2011) 5692–5696.
- Y.W. Ju, T. Inagaki, S. Ida, T. Ishihara, *J. Electrochem. Soc.* 158 (2011) B825–B830.
- E.D. Wachsman, J.S. Ahn, S. Omar, H. Yoon, J.C. Nino, *J. Power Sources* 195 (2010) 2131–2135.
- Y.Y. Chen, W.C.J. Wei, *Solid State Ionics* 177 (2006) 351–357.
- X.L. Zhou, K.N. Sun, J. Gao, S.R. Le, N.Q. Zhang, P. Wang, *J. Power Sources* 191 (2009) 528–533.
- F. Tietz, A. Mai, D. Stöver, *Solid State Ionics* 179 (2008) 1509–1515.
- J. Wang, D. Yan, J. Pu, B. Chi, L. Jian, *Int. J. Hydrogen Energy* 36 (2011) 7234–7239.
- J.M. Vohs, R.J. Gorte, *Adv. Mater.* 21 (2009) 943–956.
- J.M. Serra, H.P. Buchkremer, *J. Power Sources* 172 (2007) 768–774.
- T.H. Etzell, S.N. Flengas, *Chem. Rev.* 70 (1970) 339–376.
- S.P.S. Badwal, *Solid State Ionics* 52 (1992) 23–32.
- X. Guo, Z.L. Zhang, *Acta Mater.* 51 (2003) 2539–2547.
- X. Guo, R. Waser, *Prog. Mater. Sci.* 51 (2006) 151–210.
- C. Peters, A. Weber, B. Butz, D. Gerthsen, E. Ivers-Tiffée, *J. Am. Ceram. Soc.* 92 (2009) 2017–2024.
- F. Tietz, V.A.C. Haanappel, A. Mai, J. Mertens, D. Stöver, *J. Power Sources* 156 (2006) 20–22.
- V.A.C. Haanappel, A. Mai, J. Mertens, *Solid State Ionics* 177 (2006) 2033–2037.
- P. Hjalmarsson, M. Sogaard, M. Mogensen, *Solid State Ionics* 179 (2008) 1422–1426.
- W. Schafbauer, R. Kauert, N.H. Menzler, H.P. Buchkremer, in: R. Steinberger-Wilckens, U. Bossel (Eds.), *Proc. 8th European Solid Oxide Fuel Cell Forum*, Oberrohrdorf, Switzerland (2008), p. B0512.
- W. Schafbauer, Entwicklung und Herstellung von foliengegossenen, anoden gestützten Festoxidbrennstoffzellen, PhD Thesis, Energy & Environment 66, Forschungszentrum Jülich Zentralbibliothek, Verlag, 2010.
- T. Van Gestel, F. Han, D. Sebold, H.P. Buchkremer, D. Stöver, *Microsyst. Technol.* 17 (2011) 233–242.
- T. Van Gestel, D. Sebold, H.P. Buchkremer, D. Stöver, *J. Eur. Ceram. Soc.* 32 (2012) 9–26.
- S. Uhlenbrück, N. Jordan, D. Sebold, H.P. Buchkremer, V.A.C. Haanappel, D. Stöver, *Thin Solid Films* 515 (2007) 4053–4060.
- F.C. Fonseca, S. Uhlenbrück, R. Nedelec, H.P. Buchkremer, *J. Power Sources* 195 (2010) 1599–1604.
- P. Ried, C. Lorenz, A. Bronstrup, T. Graule, N.H. Menzler, W. Sitte, P. Holtappels, *J. Eur. Ceram. Soc.* 28 (2008) 1801–1808.
- A. Leonide, V. Sonn, A. Weber, E. Ivers-Tiffée, *J. Electrochem. Soc.* 155 (2008) B36–B41.
- R. Mücke, N.H. Menzler, H.P. Buchkremer, D. Stöver, *J. Am. Ceram. Soc.* 92 (2009) S95–S102.
- A. Mai, V.A.C. Haanappel, S. Uhlenbrück, F. Tietz, D. Stöver, *Solid State Ionics* 176 (2005) 1341–1350.
- H.S. Noh, H. Lee, B.K. Kim, H.W. Lee, J.H. Lee, J.W. Son, *J. Power Sources* 196 (2011) 7169–7174.
- D.F. Wang, J.X. Wang, C.R. He, Y.K. Tao, C. Xu, W.G. Wang, *J. Alloys Compd.* 505 (2010) 118–124.
- V.A.C. Haanappel, J. Mertens, A. Mai, *J. Fuel Cell Sci. Technol.* 3 (2006) 263–270.
- S. Hashimoto, H. Nishino, Y. Liu, K. Asano, M. Mori, Y. Funahashi, Y. Fujishiro, *J. Power Sources* 181 (2008) 244–250.